

Provided for non-commercial research and education use.  
Not for reproduction, distribution or commercial use.



This article appeared in a journal published by Elsevier. The attached copy is furnished to the author for internal non-commercial research and education use, including for instruction at the authors institution and sharing with colleagues.

Other uses, including reproduction and distribution, or selling or licensing copies, or posting to personal, institutional or third party websites are prohibited.

In most cases authors are permitted to post their version of the article (e.g. in Word or Tex form) to their personal website or institutional repository. Authors requiring further information regarding Elsevier's archiving and manuscript policies are encouraged to visit:

<http://www.elsevier.com/copyright>



Contents lists available at ScienceDirect

Physics Letters A

www.elsevier.com/locate/pla



# Classical study of the rovibrational dynamics of a polar diatomic molecule in static electric fields

Manuel Iñarrea<sup>a,\*</sup>, J. Pablo Salas<sup>a</sup>, Rosario González-Férez<sup>b,c</sup>, Peter Schmelcher<sup>d,e</sup>

<sup>a</sup> Área de Física, Universidad de la Rioja, E-26006 Logroño, Spain

<sup>b</sup> Instituto 'Carlos I' de Física Teórica y Computacional, Universidad de Granada, E-18071 Granada, Spain

<sup>c</sup> Departamento de Física Atómica, Molecular y Nuclear, Universidad de Granada, E-18071 Granada, Spain

<sup>d</sup> Theoretische Chemie, Physikalisch-Chemisches Institut, D-69120 Heidelberg, Germany

<sup>e</sup> Physikalisches Institut, Universität Heidelberg, D-69120 Heidelberg, Germany

## ARTICLE INFO

### Article history:

Received 10 August 2009  
Received in revised form 29 October 2009  
Accepted 3 November 2009  
Available online 11 November 2009  
Communicated by A.P. Fordy

### PACS:

32.60.+i  
05.45.-a  
33.20.Vq  
45.20.Jj

### Keywords:

Heteronuclear alkali dimers  
Molecular rovibrational dynamics  
Nonlinear Hamiltonian dynamics  
Chaos

## ABSTRACT

We study the classical dynamics of a polar diatomic molecule in the presence of a strong static homogeneous electric field. Our full rovibrational investigation includes the interaction with the field due to the permanent electric dipole moment and the polarizability of the molecule. Using the LiCs molecule as a prototype, we explore the stability of the equilibrium points and their bifurcations as the field strength is increased. The phase space structure and its dependence on the energy and field strength are analyzed in detail. We demonstrate that depending on the field strength and on the energy, the phase space is characterized either by regular features or by small stochastic layers of chaotic motion.

© 2009 Elsevier B.V. All rights reserved.

## 1. Introduction

Molecules exposed to external fields represent, in spite of its substantial history, a very active and promising research area with several intriguing perspectives. The recent availability of large samples of ultracold heteronuclear diatomic molecules in their absolute ground state [1,2] represents an important breakthrough in this field. These ultracold samples of polar dimers provide an ideal laboratory to study fundamental quantum processes, e.g., the many-body, scattering and chemical reactions dynamics. Several theoretical investigations indicate that external fields are unique tools to control and manipulate chemical reactions [3], collisions [4–8], their formation [9,10], or even to create quantum computing devices [11–13]. Initially, the experiments on molecules in electric fields were motivated by the possibility to understand and control molecular dynamics by modifying the orientation and alignment of the involved species [14–17]. These experimental studies have

been followed up by theoretical investigations of the impact of the external fields on the internal molecular structure, specifically the rotational dynamics [18–20]. One of the major effects for strong fields is the appearance of pendular states for which the molecule is oriented and/or aligned along the electric field axis. Traditionally, the theoretical description of the nuclear dynamics of these dimers exposed to an electric field is based on the rigid rotor approximation, neglecting the coupling between the vibrational and rotational motion, and assuming a constant dipole moment and polarizabilities for the molecule [21]. Recently, full rovibrational descriptions were performed and, in particular, the possibility to affect also the vibrational motion of the polar dimer has been demonstrated for strong field strengths and certain energy regions of the rovibrational spectrum [22–24].

In the classical framework, several studies have been dedicated to investigate the rotational dynamics of diatomic molecules in the presence of combined electrostatic and non-resonant polarized laser field. For the case of parallel fields, the analysis of the stability of the equilibrium points, their bifurcation and the evolution of the phase flow have provided a detailed picture of the classical dynamics and in particular of the influence on the ori-

\* Corresponding author.

E-mail address: manuel.inarrea@unirioja.es (M. Iñarrea).

entation of the quantum states [25]. For the general case of tilted fields, the phase space structure, the degree of classical chaos, the classical–quantum correspondence for the non-integrable case, and the phenomenon of monodromy have been investigated [26,27]. The signatures of classical and quantum chaos in the rotational dynamics of a dimer exposed to ac electric fields were studied revealing a close correspondence between classically chaotic dynamics and corresponding quantum time evolution [28]. The transition from regular motion to dynamical chaos in a classical model of a diatomic molecules driven by a circular polarized resonant IR field has been analyzed. In particular, it has been demonstrated that the transition to chaos is connected with the overlapping of vibrational–rotational nonlinear resonances and appears at rather low radiation field intensities [29,30]. The dissociation dynamics of a diatomic molecule driven by a bichromatic field has been analyzed in terms of periodic bifurcations [31]. For polyatomic molecules, it has been demonstrated that classical stationary objects, e.g., equilibria, periodic orbits, tori or manifolds, act as organizing structures for the quantum mechanical eigenstates and their identification is needed for the spectral assignment of highly excited levels [32].

The purpose of the present Letter is to investigate the classical dynamics of a heteronuclear diatomic molecule, with electronic ground state of  $^1\Sigma^+$  symmetry, exposed to a strong homogeneous static electric field. We perform a full rovibrational study, i.e., the vibration–rotation coupling is taken into account, and we include the interaction of the external field with the molecular electric dipole moment and polarizability. In particular, we analyze the equilibrium points, provide their classification and their dependence on the field strength, showing that in the strong field regime the system presents pitchfork and saddle-node bifurcations, as well as two saddle connections. The phase space structure and its evolution with the field strength and energy is studied by means of Poincaré surfaces of section. Whereas, for low-lying energies, the phase space structure presents a quite regular structure, for energies close to the dissociation threshold, it is characterized by small stochastic layers of chaotic motion. As an example we will focus on the LiCs molecule, for which we have performed several quantum studies of its rovibrational dynamics in the presence of electric fields [33–36].

The Letter is organized as follows. In Section 2, the two-dimensional Hamiltonian used to describe the dynamics of the polar dimer and the corresponding classical equations of motion are presented. The classification of the equilibrium points as a function of the field strength is provided in Section 3. Section 4 is devoted to the analysis of the phase space structure. The conclusions and outlook are provided in Section 5. Atomic units will be used throughout, unless stated otherwise.

## 2. Classical Hamiltonian and equations of motion

We employ the Born–Oppenheimer approximation to describe the dynamics of a heteronuclear dimer in its  $^1\Sigma^+$  electronic ground state in the presence of a homogeneous static electric field. Our study is focused on the field regime where perturbation theory holds for the description of the field impact on the electronic structure, whereas a nonperturbative treatment is indispensable for the corresponding nuclear dynamics. In addition, we restrict our study to a non-relativistic treatment and we take into account that the interaction of the field with the molecule is via its dipole moment and polarizability, neglecting higher order polarizability contributions. In the rotating molecule fixed frame with the coordinate origin at the center of mass of the nuclei, the classical Hamiltonian describing the nuclear motion is given by:

$$\mathcal{H} = \frac{P_R^2}{2\mu} + \frac{P_\theta^2}{2\mu R^2} + \frac{P_\phi^2}{2\mu R^2 \sin^2 \theta} + V(R, \theta), \quad (1)$$

$$V(R, \theta) = \varepsilon(R) - FD(R) \cos \theta - \frac{F^2}{2} [(\alpha_{\parallel}(R) - \alpha_{\perp}(R)) \cos^2 \theta + \alpha_{\perp}(R)], \quad (2)$$

where  $\mu$  is the reduced mass of the nuclei,  $(R, \theta, \phi)$  represent the internuclear coordinate and the Euler angles, and  $P_R$ ,  $P_\theta$  and  $P_\phi$  are the corresponding classical conjugate momenta.  $V(R, \theta)$  is an effective potential composed by the field-free adiabatic electronic potential energy curve,  $\varepsilon(R)$ , and the interaction of the electric field with the electronic dipole moment function,  $D(R)$ , and the molecular polarizability, with  $\alpha_{\parallel}(R)$  and  $\alpha_{\perp}(R)$  being the corresponding parallel and perpendicular components, respectively. The electric field is oriented parallel to the  $z$  axis in the laboratory frame with strength  $F$ .

Owing to the axial symmetry,  $P_\phi$  is conserved, note that,  $P_\phi$  is the  $z$ -component of the angular momentum. Hence, the expression (1) defines the classical Hamiltonian of a system with two degrees of freedom  $(R, \theta)$ . The present study is restricted to the  $P_\phi = 0$  case, i.e., the corresponding magnetic quantum number is zero. Hence, for  $P_\phi = 0$ , the Hamiltonian equations of motion read as

$$\begin{aligned} \dot{R} &= \frac{P_R}{\mu}, & \dot{\theta} &= \frac{P_\theta}{\mu R^2}, \\ \dot{P}_R &= \frac{P_\theta^2}{\mu R^3} - \frac{\partial \varepsilon}{\partial R} + F \frac{\partial D}{\partial R} \cos \theta \\ &\quad + \frac{F^2}{2} \left[ \left( \frac{\partial \alpha_{\parallel}}{\partial R} - \frac{\partial \alpha_{\perp}}{\partial R} \right) \cos^2 \theta + \frac{\partial \alpha_{\perp}}{\partial R} \right], \\ \dot{P}_\theta &= -\frac{\partial V(R, \theta)}{\partial \theta} \\ &= -[FD(R) + F^2(\alpha_{\parallel}(R) - \alpha_{\perp}(R)) \cos \theta] \sin \theta. \end{aligned} \quad (3)$$

Besides  $P_\phi$ , the classical dynamics of this system depends on the energy  $E = \mathcal{H}$  and on the external parameter  $F$ .

## 3. The equilibrium points

The equilibrium points of the above Hamiltonian flux are the critical points of the potential  $V(R, \theta)$  together with the conditions  $P_R = 0$  and  $P_\theta = 0$ . By substituting these conditions in Eq. (3), it yields

$$\frac{\partial \varepsilon}{\partial R} - F \frac{\partial D}{\partial R} \cos \theta - \frac{F^2}{2} \left[ \left( \frac{\partial \alpha_{\parallel}}{\partial R} - \frac{\partial \alpha_{\perp}}{\partial R} \right) \cos^2 \theta + \frac{\partial \alpha_{\perp}}{\partial R} \right] = 0, \quad (4)$$

$$[FD(R) + F^2(\alpha_{\parallel}(R) - \alpha_{\perp}(R)) \cos \theta] \sin \theta = 0. \quad (5)$$

From Eq. (5), it is clear that the equilibrium points, when they exist, appear at

$$\begin{aligned} \theta_1 &= 0, & \theta_2 &= \pi, & \text{and} \\ \cos \theta_3 &= \gamma(R) = \left[ \frac{|D(R)|}{F(\alpha_{\parallel}(R) - \alpha_{\perp}(R))} \right] \leq 1. \end{aligned}$$

Whereas the critical points associated to  $\theta = 0$  and  $\pi$  are due to the interaction of the field with the molecular dipole moment, those arising from  $\cos \theta_3 = \gamma(R)$  are due to the molecular polarizability. When these three values of  $\theta$  are substituted in (4), we obtain

$$-\frac{\partial \varepsilon}{\partial R} + F \frac{\partial D}{\partial R} + \frac{F^2}{2} \frac{\partial \alpha_{\parallel}}{\partial R} = 0, \quad (6)$$

$$-\frac{\partial \varepsilon}{\partial R} - F \frac{\partial D}{\partial R} + \frac{F^2}{2} \frac{\partial \alpha_{\parallel}}{\partial R} = 0, \quad (7)$$

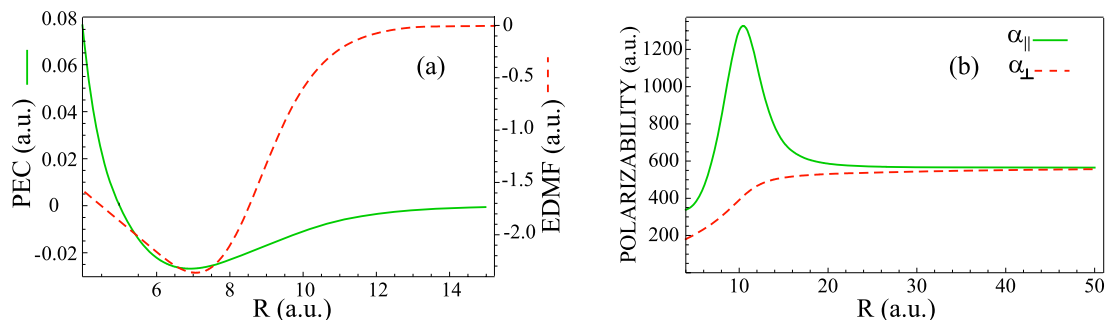


**Fig. 1.** (a) Electronic potential energy curve and electronic dipole moment function of LiCs. (b) Parallel  $\alpha_{\parallel}(R)$  and perpendicular  $\alpha_{\perp}(R)$  components of the molecular polarizability.

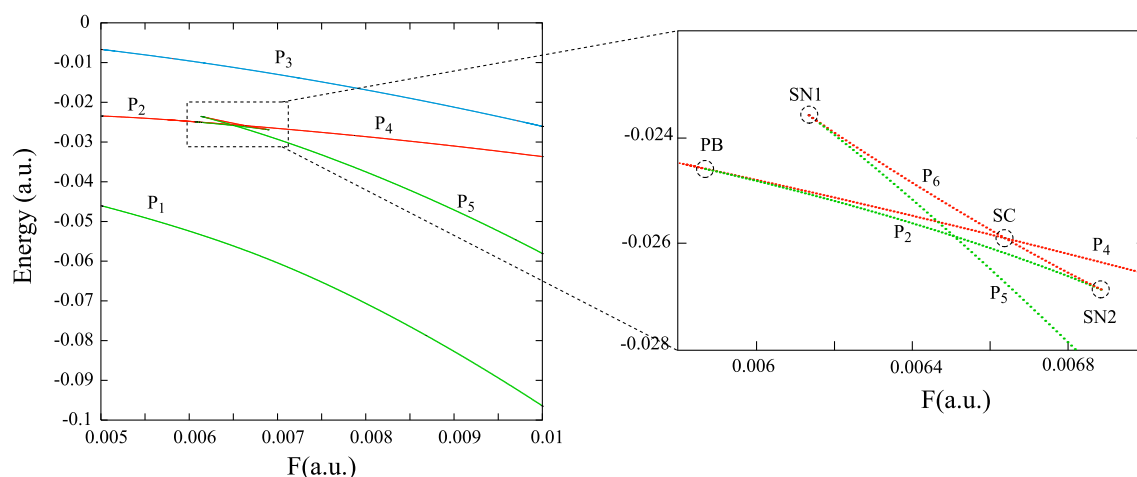


**Fig. 2.** Evolution of the energy of the critical points of the effective potential  $V(R, \theta)$  as a function of the electric field  $F$ . Red, green and blue colors indicate that the corresponding critical point is a saddle point, a (relative) minimum or a (relative) maximum, respectively. (For interpretation of the references to color in this figure legend, the reader is referred to the web version of this Letter.)

$$-\frac{\partial \varepsilon}{\partial R} + F \frac{\partial D}{\partial R} \gamma(R) + \frac{F^2}{2} \left[ \left( \frac{\partial \alpha_{\parallel}}{\partial R} - \frac{\partial \alpha_{\perp}}{\partial R} \right) \gamma(R)^2 + \frac{\partial \alpha_{\perp}}{\partial R} \right] = 0. \quad (8)$$

Since the analytical forms of  $\varepsilon(R)$ ,  $D(R)$ ,  $\alpha_{\parallel}(R)$  and  $\alpha_{\perp}(R)$  are not known, it is impossible to provide close expressions of the roots of Eqs. (6), (7) and (8) as a function of the field strength. Thus, a numerical study is required to obtain these roots and to investigate the nature of the corresponding critical points.

We have taken the  ${}^7\text{Li}^{133}\text{Cs}$  dimer as a prototype system for this study. The potential energy curve  $\varepsilon(R)$  [37], electric dipole moment function  $D(R)$  [38], and the polarizabilities  $\alpha_{\parallel}(R)$  and  $\alpha_{\perp}(R)$  [39] of this system are plotted in Fig. 1. The evolution of the critical points is illustrated by the diagram of their energy as a function of  $F$  presented in Fig. 2, where the existence of several bifurcations is recognized. For  $F < 0.005867$  a.u., we encounter three critical points:  $P_1$  is a minimum,  $P_2$  a saddle point and  $P_3$  a maximum. The contour plot of  $V(R, \theta)$  for  $F = 2.5 \times 10^{-3}$  a.u. is depicted in Fig. 3(a), where depending on the value of the energy two different regions of motion are distinguished. For illustrative purposes, the potentials have been plotted for  $-\pi \leq \theta \leq \pi$ , and not only in the interval of definition of the polar angle  $[0, \pi]$ . When the energy  $E$  is below the energy of the saddle point  $P_2$ , the molecule is trapped into the potential energy well around  $\theta = \pi$ , in such a way that, the field prevents the molecule from describing complete rotations. Thence, the molecule can eventually be oriented along the opposite electric field direction, as it corresponds to the pendular states of dimers with a negative electric dipole moment. Note that, as  $F$  increases in this interval, the depth of the potential well in-

creases. In contrast, when the energy surpasses the energy of  $P_2$ , the electric field is not able to trap the molecule and its motion describes complete rotations. Moreover, the polarizability creates an “energy hill” (the maximum  $P_3$ ) which, in fact, prevents the molecular bond  $R$  from reaching large values unless across two narrow channels located along the  $\theta = 0$  and  $\pi$  directions (see Fig. 4). For comparison, Fig. 3(b) shows the shape of the effective potential excluding the interaction with the molecular polarizability. In this case, there only exist the critical points  $P_1$  and  $P_2$  and the corresponding structures in phase space remain for any value of the electric field strength.

Fig. 5 illustrates the evolution of the potential energy surface  $V(R, \theta)$  for  $0.0055$  a.u.  $\leq F \leq 0.008$  a.u., i.e., in the regime shown in the subset of Fig. 2 where several bifurcations take place. The saddle point  $P_2$  appearing in Fig. 5(a), undergoes a pitchfork bifurcation for  $F \approx 0.005867$  a.u., which is denoted by PB in Fig. 2,  $P_2$  becomes a minimum and gives rise to two saddle points  $P_4$ . The separatrix passing through these saddles  $P_4$  surrounds a new potential energy well centered at  $P_2$ , see Fig. 5(b). When the electric field is slightly increased reaching the value  $F \approx 0.006133$  a.u., the first saddle-node bifurcation takes place, SN1 in Fig. 2. Two new critical points appear, a minimum  $P_5$  and a saddle point  $P_6$ , along the  $\theta = 0$  axis, see Fig. 5(c). From this bifurcation  $V(R, \theta)$  shows a new potential energy well centered at the minimum  $P_5$ . For a further increase of  $F$ , the separatrices passing through  $P_4$  and  $P_6$  approach one another and they merge at  $F \approx 0.006637$  a.u. where a saddle-connection, SC, occurs, see Fig. 5(d). As we observe in Fig. 5(e), after passing this field strength, the two separatrices interchange the minimum they surround. A second saddle-node

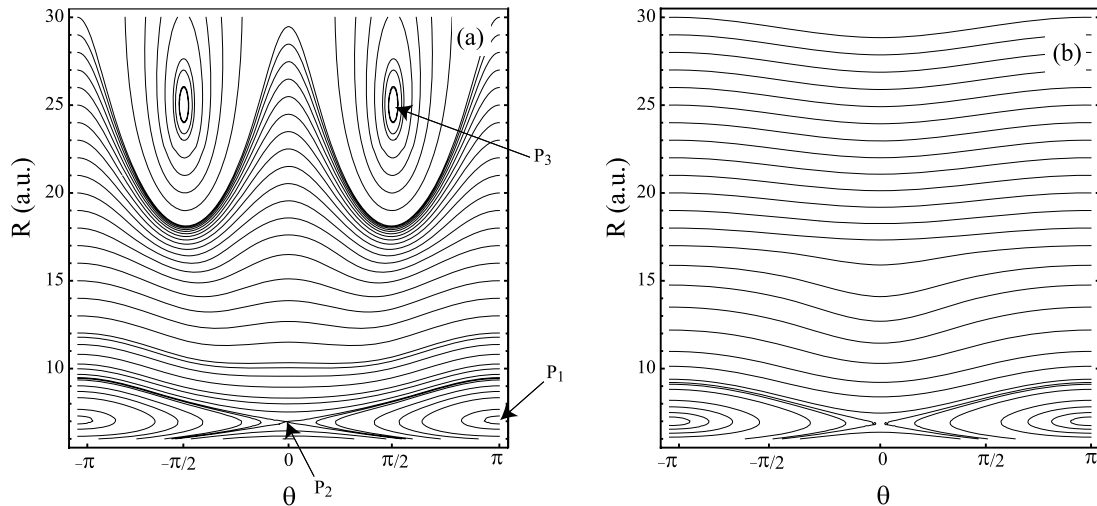


**Fig. 3.** Equipotential curves of the effective potential  $V(\theta, R)$  with polarizability (a) and without polarizability (b). Both figures are calculated for the same electric field strength  $F = 0.0025$  a.u.

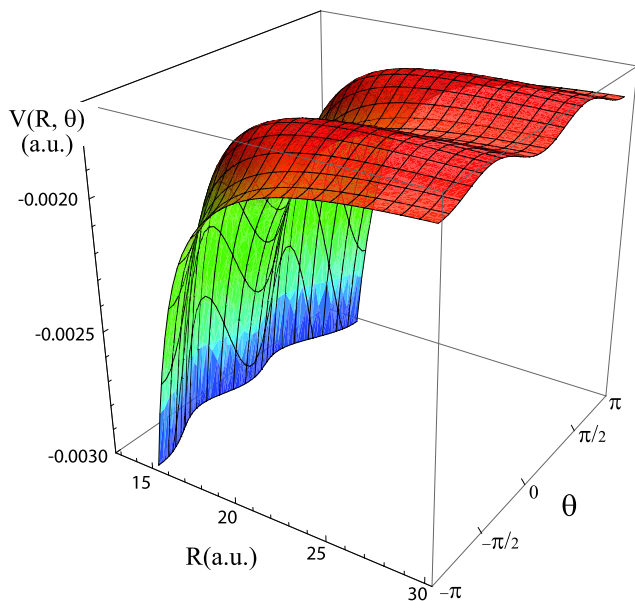


**Fig. 4.** Effective potential surface  $V(\theta, R)$  for the electric field strength  $F = 0.0025$  a.u.

bifurcation, SN2, occurs for  $F \approx 0.006893$  a.u., where the minimum  $P_2$  and the saddle  $P_6$  come into coincidence and both disappear (see Fig. 5(f)). From this value of  $F$  on, the structure of  $V(R, \theta)$  remains unchanged. This chain of bifurcations can be understood as the route to the appearance of a new kind of oscillatory orbits around  $P_5$ . In contrast to the vibrational orbits around  $P_1$ , in this new oscillatory mode the molecule is mainly aligned along the  $\theta = 0$  direction. At such strong fields, the dynamics is dominated by the interaction of the field with the polarizability. As a direct consequence, the dimer presents this *anomalous* molecular orientation parallel to the field direction, i.e., opposite to the orientation due to the interaction with the dipole moment.

#### 4. Evolution of the phase space

In this section we get a deeper physical insight of the phase space structure of this system by analyzing the Poincaré surfaces of section [40] as a function of the field strength  $F$  and the energy  $E$ . We define the surface of section by the intersection of the phase trajectories with the  $(\theta, P_\theta)$ -plane for  $P_R = 0$ . With this selection

we ensure that all the orbits (both rotational and oscillatory) will cross it at any time, i.e., it is guaranteed that this surface of section is transverse to the Hamiltonian flux [41]. They are generated by the numerical integration of the Hamiltonian equations of motion (3) using an explicit Runge–Kutta algorithm of eighth order with step size control and dense output [42].

For the Hamiltonian (1) and  $P_\phi = 0$ , the region in the  $(\theta, P_\theta)$ -plane defining these Poincaré surfaces of section is determined by those values of  $P_\theta$  satisfying

$$P_\theta = \pm \sqrt{2\mu R} \left\{ E - \varepsilon(R) + FD(R) \cos \theta + \frac{F^2}{2} [(\alpha_{\parallel}(R) - \alpha_{\perp}(R)) \cos^2 \theta + \alpha_{\perp}(R)] \right\}^{1/2}. \quad (9)$$

Therefore, the limits of the surface of section correspond to the maximum and minimum values of  $P_\theta$  satisfying this equation. The initial conditions have been chosen inside the region limited by these extreme points, which were computed numerically. Note that, to get a better visualization of the different phase space structures, the surfaces of section have been plotted for  $0 \leq \theta \leq 2\pi$ , and not only in the interval of definition of the polar angle  $[0, \pi]$ .

##### 4.1. Phase space structure: normal modes

In Fig. 6(a) we show the surface of section for an electric field strength  $F = 2.5 \times 10^{-4}$  a.u. and an energy of  $E = -0.02641$  a.u., the corresponding potential energy surface has a similar structure to the case discussed in Fig. 3(a). Since this energy is below the energy of the saddle point  $P_2$ , the molecule is trapped inside the potential well of the minimum  $P_1$ . All the orbits are ordered forming invariant KAM tori around the stable fixed point located at  $(\theta, P_\theta) = (\pi, 0)$ . As can be analytically checked in (3), this fixed point corresponds to a pure vibrational rectilinear periodic orbit along the negative  $z$  axis ( $\theta = \pi$ ). In Fig. 7 this periodic orbit  $O_{V1}$  and representative quasiperiodic orbits around it are presented.

A complementary vision of the phase space structure is provided by the surface of section in the  $(R, P_R)$ -plane for  $\theta = \pi$ . In this case, the allowed region is limited by the equation

$$P_R = \pm \sqrt{2\mu[E - V(R, \pi)]}. \quad (10)$$

It is worth noting that the rectilinear orbit  $O_{V1}$  is tangent to the flux in this Poincaré map and it corresponds to the curves (10).

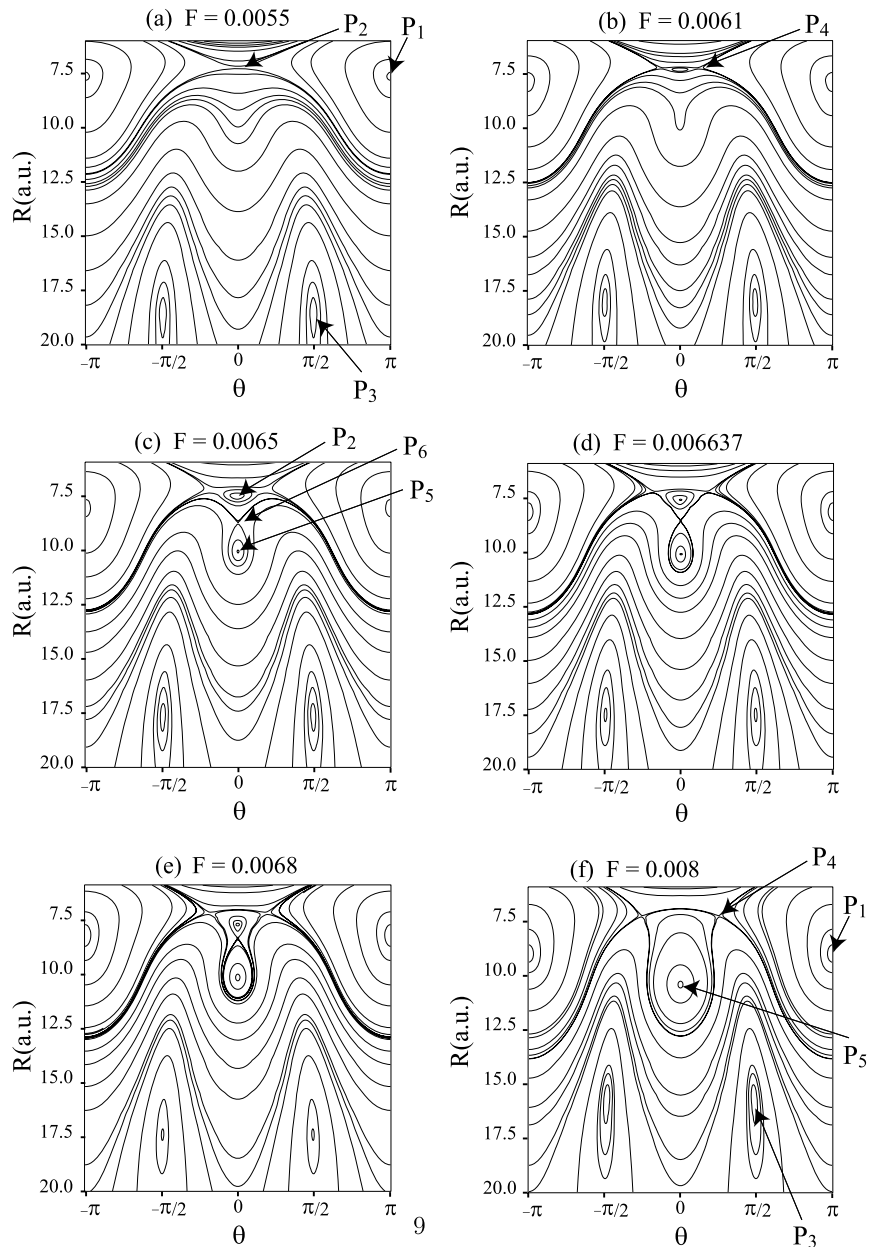


Fig. 5. Evolution of the equipotential curves of the potential  $V(\theta, R)$  as a function of the electric field  $F$ .

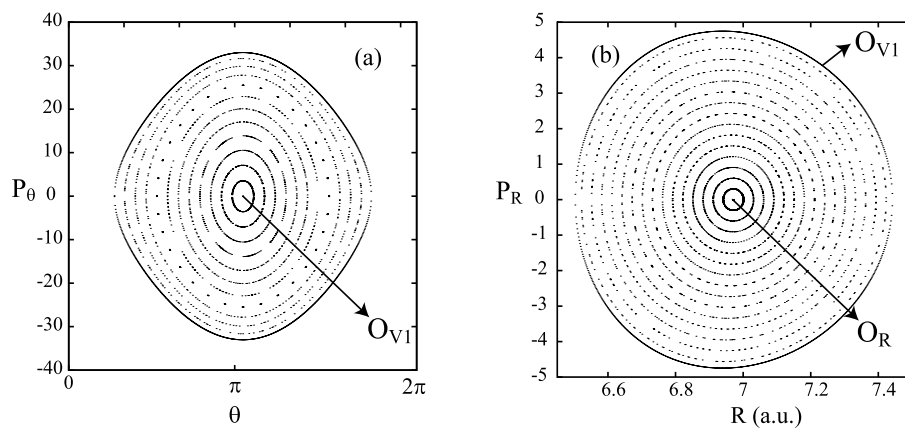
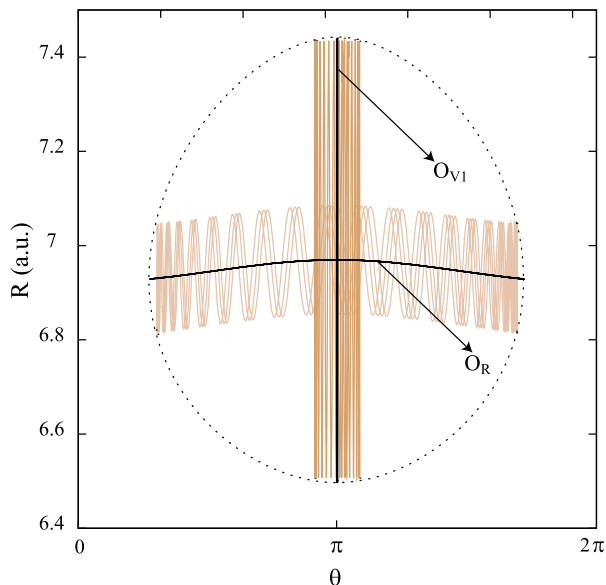


Fig. 6. Poincaré surfaces of section for  $P_R = 0$  (a) and for  $\theta = \pi$  (b). Both figures are calculated for an electric field strength  $F = 0.00025$  a.u. and an energy  $E = -0.02641$  a.u. See the text for a more detailed explanation.



**Fig. 7.** The black solid lines are the rectilinear orbits  $O_{V1}$  and  $O_R$ . Examples of quasiperiodic orbits around these periodic orbits are also shown. The dotted line is the equipotential curve of electric field strength  $F = 0.00025$  a.u. and an energy  $E = -0.02641$  a.u.

This surface of section for the same values of  $E$  and  $F$  is shown in Fig. 6(b), where a similar phase space structure as in Fig. 6(a) is observed. The rectilinear orbit  $O_{V1}$  in the center of Fig. 6(a) is now the limit of the surface of section of Fig. 6(b). This surface of section is composed of concentric orbits around a central fixed point associated to a new periodic orbit of arch-like type  $O_R$ , which is also presented in Fig. 7. In the surface of section with  $P_R = 0$  (Fig. 6(a)) this periodic orbit  $O_R$  is located on the  $P_\theta$  axis with  $\theta = \pi$  near the limit of the surface of section. Due to the small variation of the radial coordinate  $R$ , this orbit is almost tangent to the flux, which explains why it is not visible at a glance in the  $P_R = 0$  Poincaré map of Fig. 6(a). From these two different phase plots of Figs. 6(a) and 6(b), we deduce that the phase space is organized around  $O_{V1}$  and  $O_R$ . Then, the closer a quasiperiodic orbit is to  $O_{V1}$  the larger its orientation is along the negative  $z$  axis. On the other hand, the quasiperiodic orbits near  $O_R$  show an arch-like shape, see Fig. 7. Let us remark that the periodic orbits  $O_{V1}$  and  $O_R$  are, respectively, the radial and the angular normal modes of the system [43].

When the energy of the system is larger than the energy of the saddle point  $P_2$ , the molecule is not trapped into the potential well of the minimum  $P_1$  and can, eventually, describe complete rotations. To illustrate this phenomenon we have analyzed this system for the same field strength,  $F = 2.5 \times 10^{-4}$  a.u., and an energy  $E = -10^{-4}$  a.u. above the saddle point  $P_2$ . The surfaces of section in the planes  $(\theta, P_\theta)$  for  $P_R = 0$  and  $(R, P_R)$  for  $\theta = \pi$  are shown in Figs. 8(a) and 8(b), respectively. Compared to the case previously discussed, the  $(R, P_R)$  surface of section shows a similar structure to the one presented in Fig. 6(b), but for the  $(\theta, P_\theta)$  surface of section significant modifications are encountered (see Figs. 6(a) and 8(a)). In the present dynamics, two unstable fixed points located at  $(\theta, P_\theta) = (0, 0)$  and  $(2\pi, 0)$  appear, they correspond to another pure vibrational rectilinear ( $\theta = 0$ ) periodic orbit along the positive  $z$  axis, which can also be analytically checked in Eq. (3). In this orbit, labeled as  $O_{V2}$ , the electric dipole moment of the molecule is aligned parallel to the electric field (see Figs. 8(c) and 8(d)). These two unstable fixed points are connected by a separatrix that encloses the curves of the oscillatory type motions. Outside this separatrix, there is a family of curves which sweep out the angle  $\theta$  from 0 to  $2\pi$ , they correspond to complete

(quasiperiodic) molecular rotations. To obtain a global vision of the different motions that characterize the dynamics of this system, in Figs. 8(c) and 8(d) the periodic orbits  $O_{V1}$ ,  $O_{V2}$  and  $O_R$  are depicted, as well as two representative quasiperiodic orbits. Finally, note that the surfaces of section of Fig. 8 show regular behavior which indicates that, even for energies above the saddle point  $P_2$ , the system is near integrable.

#### 4.2. Dynamics close to the dissociation threshold

Having explored the fundamental structures in phase space, we investigate their evolution as a function of the energy. Fig. 9 shows a gallery of surfaces of section in the energy interval  $-10^{-4}$  a.u.  $\leq E \leq -7 \times 10^{-5}$  a.u. and for  $F = 5 \times 10^{-4}$  a.u. Since all the changes in the structure of the surface of section take place in the oscillatory region, these plots are restricted to the interval  $-30$  a.u.  $\leq P_\theta \leq 30$  a.u. The larger is the energy, the more complex is the phase space shown in Fig. 9. By the increase of the field strength, the separatrix passing through  $O_{V2}$  in Fig. 8, is replaced by a thin stochastic layer of chaotic motion, see Fig. 9(a). In this small layer, the motion of the molecule alternates in a random way between complete rotations in both directions and oscillations of large amplitude. Besides this tiny stochastic layer, the rest of the phase space remains regular, appearing several islands of resonances for a larger energy in Fig. 9(b).

For a further increase of the energy, two bifurcations take place which provoke a change on the stability of the periodic orbits  $O_{V1}$  and  $O_{V2}$ . For an energy close to  $E = -7.3 \times 10^{-5}$  a.u., see Figs. 9(c)–(d), the periodic vibrational rectilinear orbit  $O_{V2}$ , initially unstable, suffers a period-doubling bifurcation [44] becoming stable and giving rise to two new unstable fixed points. The separatrix passing through these unstable points surrounds new quasiperiodic motions around  $O_{V2}$ . They are oscillations of small amplitude around the direction of the electric field, that is, around the positive  $z$  axis. In this way, these new oscillatory motions are different from those ones existing around the periodic orbit  $O_{V1}$ , in which the molecule oscillate around the opposite direction of the field. For an energy close to  $E = -7.14 \times 10^{-5}$  a.u. the second bifurcation takes place. This new bifurcation is again a period-doubling one: from the rectilinear orbit  $O_{V1}$ , which becomes unstable, emanate two new stable fixed points (see Fig. 9(d)–(e)). These fixed points correspond to a new oscillatory periodic motion of the molecule around the opposite direction of the field.

As the energy is further increased, see Fig. 9(f)–(g), a small stochastic layer appears in the vicinity of the new separatrix passing through  $O_{V1}$  and the amount and the size of the islands of resonances increase. However, the phase space structure of the system remains qualitatively the same until the dissociation threshold is reached.

The dissociation energy threshold can be obtained by employing  $R \rightarrow \infty$  and  $P_R \rightarrow 0$ ,  $P_\theta \rightarrow 0$  in the Hamiltonian. Under these conditions and since  $\lim_{R \rightarrow \infty} \varepsilon(R) = 0$ ,  $\lim_{R \rightarrow \infty} D(R) = 0$ , the Hamiltonian (1) takes the form

$$\mathcal{H} = -\frac{F^2}{2} \left[ \left( \lim_{R \rightarrow \infty} \alpha_{\parallel}(R) - \lim_{R \rightarrow \infty} \alpha_{\perp}(R) \right) \cos^2 \theta + \lim_{R \rightarrow \infty} \alpha_{\perp}(R) \right]. \quad (11)$$

In the dissociation limit  $\alpha_{\parallel} = \alpha_{\perp} = \alpha$  and Eq. (11) yields the energy of the dissociation threshold  $E_d$  for  $\theta = 0$  or  $\pi$ :

$$E_d = -\frac{F^2}{2} \lim_{R \rightarrow \infty} \alpha(R) = -\frac{F^2}{2} (\alpha_{Li} + \alpha_{Cs}). \quad (12)$$

Note that the first orbits to dissociate are the periodic vibrational rectilinear motions  $O_{V1}$ ,  $O_{V2}$  and the quasiperiodic orbits surrounding them because, these orbits are localized along the dis-

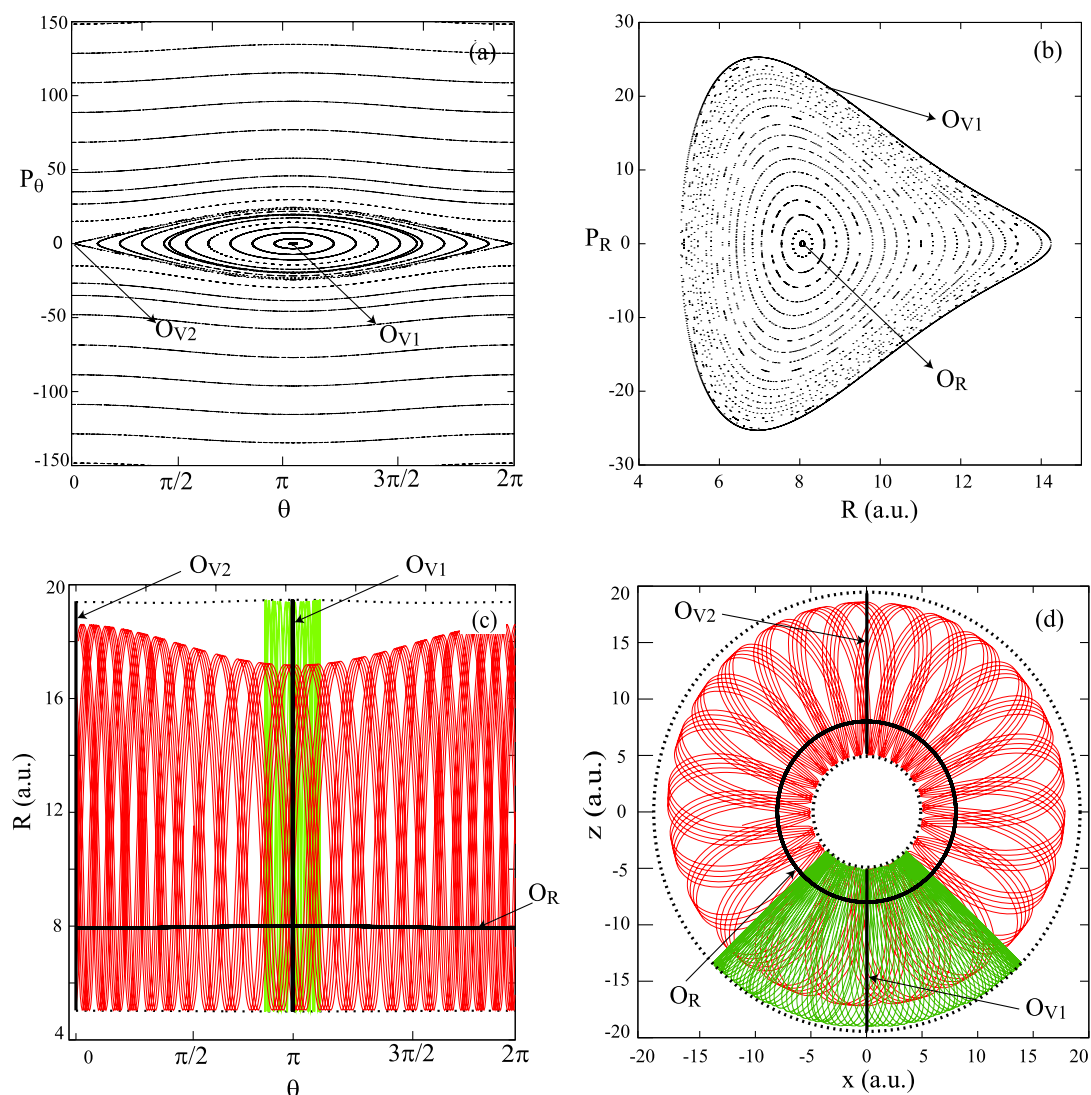


**Fig. 8.** Upper figures: Poincaré surfaces of section  $P_R = 0$  (panel (a)) and  $\theta = \pi$  (panel (b)). Lower figures: The solid black lines are the periodic orbits  $O_{V1}$ ,  $O_{V2}$  and  $O_R$ . Examples of oscillatory and rotational quasiperiodic orbits around  $O_{V1}$  and  $O_R$  are also shown. The dotted lines are the equipotential curves of energy  $E = -1 \times 10^{-4}$  a.u. Note that in (d) Cartesian coordinates  $x = R \sin \theta$  and  $z = R \cos \theta$  are used. All figures are for an electric field strength  $F = 0.00025$  a.u. and an energy  $E = -1 \times 10^{-4}$  a.u.

sociation channels  $\theta = 0$  and  $\pi$ . This phenomenon is observed in Fig. 9(h), where those orbits with  $\theta$  close to 0 and  $\pi$  are the first to disappear. Moreover, the atomic polarizabilities lead to a decrease of the dissociation energy to a nonzero negative value, which depends on the electric field strength  $F$  as well as on the atoms polarizabilities. For example, for the value  $F = 5 \times 10^{-4}$  a.u., we obtain that  $E_d = -7.065 \times 10^{-5}$  a.u., which is very close to the energy of Figs. 9(g)–(h).

It is interesting to note that for energies close or greater than  $E_d$ , quasiperiodic orbits near the periodic ones  $O_{Vi}$  have a large extension along the  $R$  coordinate and are very narrow in the  $\theta$  angle. Moreover, the numerical computation of such orbits shows that the molecule spends most of the time in regions with large values of  $R$  far from the potential well. This behavior is depicted in Fig. 10 and it is in very good agreement with the probability densities obtained from quantum calculations [36]. Let us elaborate on this last point somewhat more. The last vibrational band  $\nu = 54$  of the  ${}^7\text{Li}{}^{133}\text{Cs}$  dimer has two rotational excitations with rotational quantum number  $J = 0$  and 1. Both states have a large extension, the expectation value for the vibrational coordinate  $\langle R \rangle$  is 50.24 and 52.52 a.u. for the level with  $J = 0$  and 1, respectively. Even more, around 89% of their probability density is located at

$R > 30$  a.u. By increasing the electric field strength, the rotational and vibrational dynamics are influenced. In the strong field regime, these two levels show a significant orientation antiparallel to the field axis, and their probability density is located in the region with angles close to  $\theta = \pi$ . In addition, their vibrational motions are squeezed to minimize the energy, and for  $F = 3.4 \times 10^{-4}$  it was found  $\langle R \rangle = 28.13$  and 30.96 a.u., for the levels with  $J = 0$  and 1, respectively.

## 5. Conclusions

In the present work, we have investigated the classical rovibrational dynamics of the alkali polar dimer LiCs in its electronic ground state in the presence of a strong static homogeneous electric field, in the framework of the Born–Oppenheimer approximation. We have taken into account the interaction of the molecule with the field due to both, its permanent electric dipole moment and its polarizability. Due to the axial symmetry of the system, the component  $P_\phi$  of the angular momentum is conserved, and hence, the system has two degrees of freedom. Our study focuses on the case  $P_\phi = 0$ , that is, a zero magnetic quantum number. We have

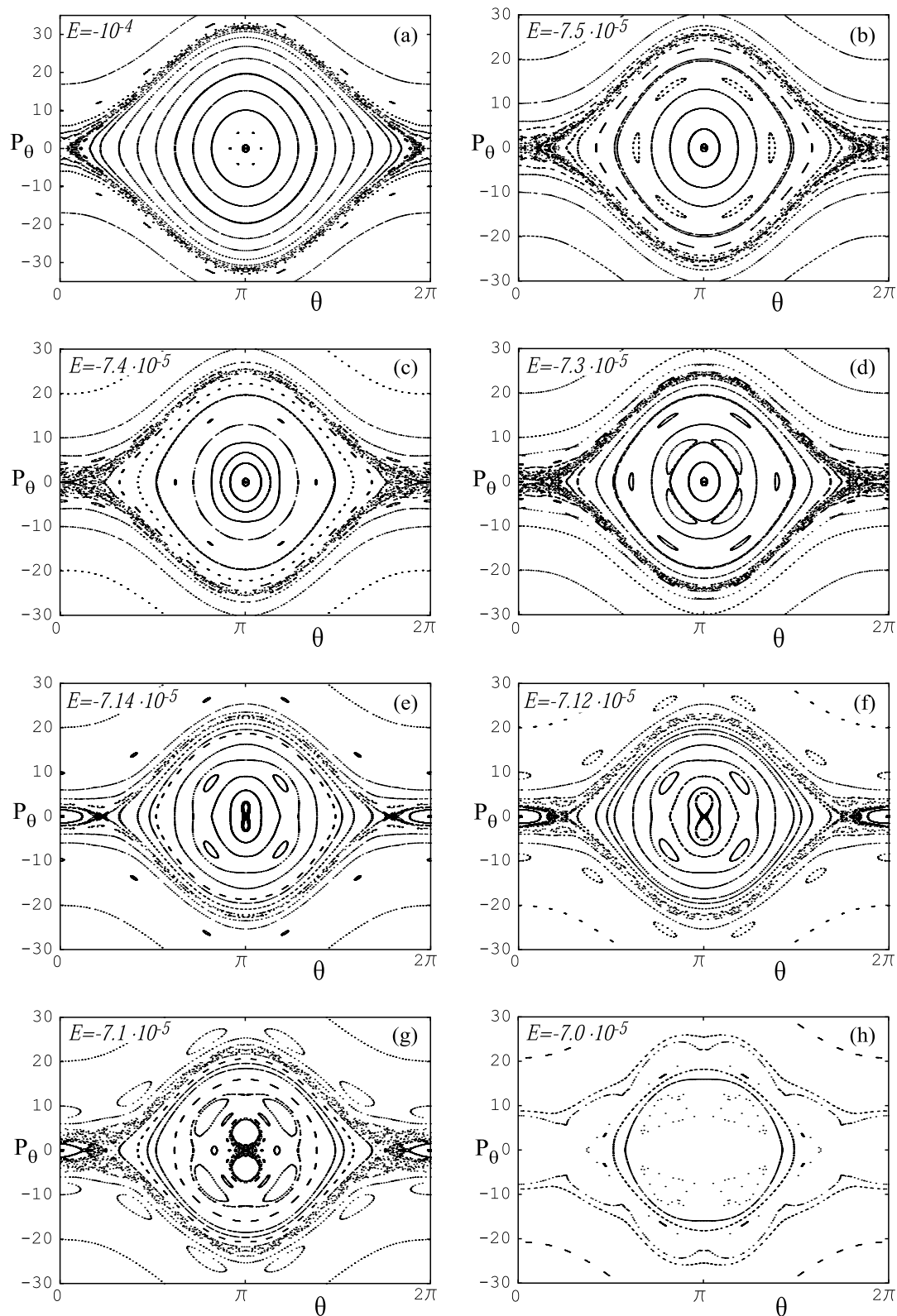
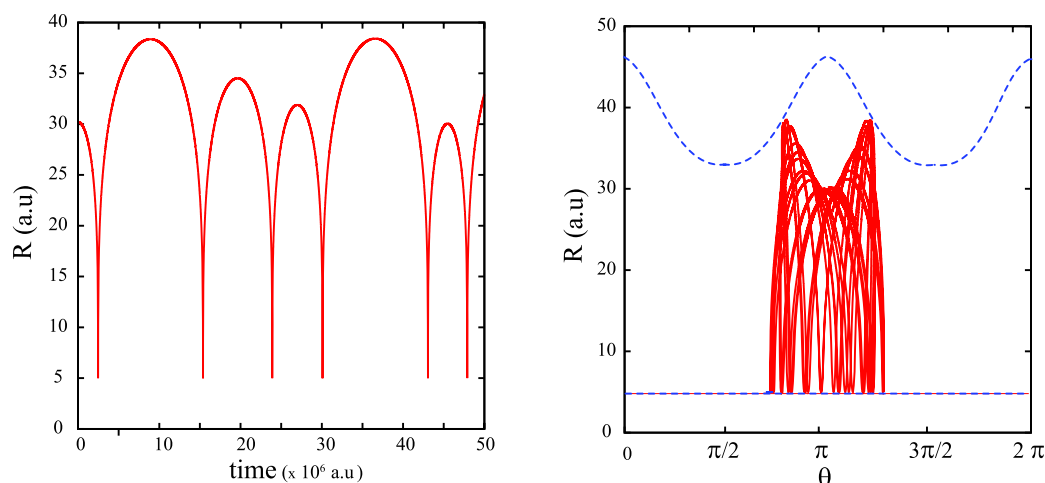


Fig. 9. Evolution of the Poincaré surfaces of section  $P_R = 0$  as a function of the energy  $E$  for an electric field strength  $F = 5 \times 10^{-4}$  a.u.

found that, for strong electric fields or energies close to the dissociation threshold, the molecular polarizability of the dimer cause relevant effects on the system dynamics. Although this work is focused in the LiCs dimer, let us point out the general validity of our results.

The evolution of the potential energy surface and the corresponding critical points of the system as a function of the electric field strength have been explored. For increasing electric field, the potential energy surface suffers a sequence of bifurcations, that give rise to new critical points. Some of these critical points corre-



**Fig. 10.** Temporal evolution of the  $R$  coordinate of the orbit with initial conditions  $\theta = \pi$ ,  $R = 45$  a.u.,  $P_R = 0$  and energy close to the dissociation threshold. The dotted blue line in the right hand side figure is the equipotential energy curve. (For interpretation of the references to color in this figure legend, the reader is referred to the web version of this Letter.)

spond to system equilibria where the orientation of the molecule is aligned parallel to the electric field.

By means of suitable Poincaré surfaces of section, we have also analyzed the evolution of the system phase space as a function of the energy. For small energy values, the phase space is regular with quasiperiodic motions organized around three stable periodic orbits: the two nonlinear normal modes (one of pure vibrational type and another of oscillatory type) and a complete rotation for larger energies. For energy values close to the dissociation threshold, the system loses part of its regularity. A small stochastic layer of chaotic motions appears in the vicinity of the separatrix which keeps apart the oscillatory motions from the complete rotations. In this tiny chaotic region, the dimer alternates randomly between complete rotations in both directions and oscillations of large amplitude. In this range of high energies, we have also found that the phase space suffers two successive bifurcations, in one of which the previously unstable periodic pure vibrational rectilinear motion parallel to the direction of the electric field becomes a stable periodic orbit, leading to new quasiperiodic oscillations of small amplitude around this direction. Thus, for energies close to the dissociation threshold the molecule can also be oriented in an anomalous stable way parallel to the electric field direction.

With regards to the dissociation of the molecule, there exist two dissociation channels located along the direction of the electric field, as the first orbits to dissociate are the two periodic pure vibrational rectilinear motions and the quasiperiodic orbits surrounding them.

## Acknowledgements

Financial support by the Spanish projects FIS2008-02380 and MTM2008-03818 (MEC) and FQM-0207, FQM-481 and P06-FQM-01735 (Junta de Andalucía) is gratefully appreciated.

## References

- [1] K.-K. Ni, S. Ospelkaus, M.H.G. de Miranda, A. Pe'er, B. Neyenhuis, J.J. Zirbel, S. Kotochigova, P.S. Julienne, D.S. Jin, J. Ye, *Science* 322 (2008) 231.
- [2] J. Deiglmayr, A. Grochola, M. Repp, K. Mörtlbauer, C. Glück, J. Lange, O. Dulieu, R. Wester, M. Weidemüller, *Phys. Rev. Lett.* 101 (2008) 133004.
- [3] R.V. Krems, *Phys. Chem. Chem. Phys.* 10 (2008) 4079.
- [4] R.V. Krems, *Phys. Rev. Lett.* 96 (2006) 123202.
- [5] T.V. Tscherbul, R.V. Krems, *J. Chem. Phys.* 125 (2006) 194311.
- [6] A.V. Avdeenkov, M. Kajita, J.L. Bohn, *Phys. Rev. A* 73 (2006) 022707.
- [7] A.V. Gorshkov, P. Rabl, G. Pupillo, A. Micheli, P. Zoller, M.D. Lukin, H.P. Büchler, *Phys. Rev. Lett.* 101 (2008) 073201.
- [8] C. Ticknor, *Phys. Rev. Lett.* 100 (2008) 133202.
- [9] R. González-Férez, M. Weidemüller, P. Schmelcher, *Phys. Rev. A* 76 (2007) 023402.
- [10] R. González-Férez, M. Mayle, P. Schmelcher, *Europhys. Lett.* 78 (2007) 53001.
- [11] D. DeMille, *Phys. Rev. Lett.* 88 (2002) 067901.
- [12] A. André, D. DeMille, J.M. Doyle, M.D. Lukin, S.E. Maxwell, P. Rabl, R.J. Schoelkopf, P. Zoller, *Nat. Phys.* 2 (2006) 636.
- [13] S.F. Yelin, K. Kirby, R. Côté, *Phys. Rev. A* 74 (2006) 050301.
- [14] P.R. Brooks, *Science* 193 (1976) 11.
- [15] S. Stolte, *Atomic and Molecular Beam Methods*, vol. 1, Oxford University Press, New York, 1988.
- [16] H.J. Loesch, A. Remscheid, *J. Chem. Phys.* 93 (1990) 4779.
- [17] B. Friedrich, D.R. Herschbach, *Nature* 353 (1991) 412.
- [18] J.M. Rost, J.C. Griffin, B. Friedrich, D.R. Herschbach, *Phys. Rev. Lett.* 68 (1992) 1299.
- [19] B. Friedrich, D. Herschbach, *Phys. Rev. Lett.* 74 (1995) 4623.
- [20] B. Friedrich, D. Herschbach, *J. Phys. Chem. A* 103 (1999) 10280.
- [21] K. von Meyenn, *Z. Physik* 231 (1970) 154.
- [22] R. González-Férez, P. Schmelcher, *Phys. Rev. A* 69 (2004) 023402.
- [23] R. González-Férez, P. Schmelcher, *Phys. Rev. A* 71 (2005) 033416.
- [24] R. González-Férez, P. Schmelcher, *Europhys. Lett.* 72 (2005) 555.
- [25] J.P. Salas, *Eur. Phys. J. D* 41 (2007) 95.
- [26] C.A. Arango, W.W. Kennerly, G.S. Ezra, *J. Chem. Phys.* 122 (2005) 184303.
- [27] C.A. Arango, W.W. Kennerly, G.S. Ezra, *Chem. Phys. Lett.* 392 (2004) 486.
- [28] N. Moiseyev, H.J. Horsch, B. Mirbach, *Z. Phys. D* 29 (1994) 125.
- [29] A. Kolovsky, *Phys. Lett. A* 157 (1991) 474.
- [30] G.P. Berman, E.N. Bulgakov, D.D. Holm, *Phys. Rev. A* 52 (1995) 3074.
- [31] S. Huang, C. Chandre, T. Uzer, *J. Chem. Phys.* 128 (2008) 174105.
- [32] S.C. Farantos, R. Schinke, H. Guo, M. Joyeux, *Chem. Rev.* 109 (2009) 4248.
- [33] R. González-Férez, M. Mayle, P. Schmelcher, *Chem. Phys.* 329 (2006) 203.
- [34] M. Mayle, R. González-Férez, P. Schmelcher, *Phys. Rev. A* 75 (2007) 013421.
- [35] P. Sánchez-Moreno, R. González-Férez, P. Schmelcher, *Phys. Rev. A* 76 (2007) 053413.
- [36] R. González-Férez, P. Schmelcher, *New J. Phys.* 11 (2009) 055013.
- [37] P. Staunum, A. Pashov, H. Knockel, E. Tiemann, *Phys. Rev. A* 75 (2007) 042513.
- [38] M. Aymar, O. Dulieu, *J. Chem. Phys.* 122 (2005) 204302.
- [39] J. Deiglmayr, M. Aymar, R. Wester, M. Weidemüller, O. Dulieu, *J. Chem. Phys.* 129 (2008) 064309.
- [40] G. Birkhoff, *Dynamical Systems*, American Mathematical Society, New York, 1927.
- [41] H.R. Dullin, A. Wittek, *J. Phys. A: Math. Gen.* 28 (1995) 7157.
- [42] S.N.E. Hairer, G. Wanner, *Solving Ordinary Differential Equations I. Nonstiff Problems*, second ed., Springer Series in Computational Mathematics, Springer-Verlag, New York, 1993.
- [43] A. Weinstein, *Inventiones Math.* 20 (1973) 47.
- [44] R. Barrio, F. Blesa, *Chaos, Solitons Fractals* 41 (2009) 560.